Mass estimation of a quadcopter using IMU data

Du Ho, Jonas Linder, Gustaf Hendeby and Martin Enqvist

Book Chapter

Part of: 2017 International Conference on Unmanned Aircraft Systems (ICUAS), June 13-16, 2017, Miami, FL, USA, Eds , 2017, pp. 1260-1266. ISBN: 9781509044955
DOI: https://dx.doi.org/10.1109/ICUAS.2017.7991417

Mass estimation of a quadcopter using IMU data

Du Ho[1], Jonas Linder[1], Gustaf Hendeby[1] and Martin Enqvist[1]

Abstract— **In this paper, an approach to estimate the mass of a quadcopter using only inertial measurements and pilot commands is presented. For this purpose, a lateral dynamic model describing the relation between the roll rate and the lateral acceleration is formulated. Due to the quadcopter's inherent instability, a controller is used to stabilize the system and the data is collected in closed loop. Under the effect of feedback and disturbances, the inertial measurements used as input and output are correlated with the disturbances, which complicates the parameter estimation. The parameters of the model are estimated using several methods. The simulation and experimental results show that the instrumental-variable method has the best potential to estimate the mass of the quadcopter in this setup.**

I. Introduction

A quadcopter is a small unmanned aerial vehicle (UAV) that uses four equally spaced rotors. The propellers have fixed pitch and are arranged in counter-rotating pairs, which gives the quadcopter a simpler mechanical structure and easier maintenance than a conventional helicopter. Each rotor produces a thrust and a torque, which combined create the main thrust, and the roll, pitch and yaw torques. Therefore, due to the high degree of freedom, the quadcopters have the ability to perform quick and complex maneuvers.

Because of these two main advantages, the quadcopter has become a standard platform in the robotics research society. Quadcopters can carry a variety of payloads depending on the requirements of the tasks. Hence, single and cooperating quadcopters have been used for a wide range of applications, e.g., for surveillance, search and rescue [1] and exploring and mapping 3-D environments [2] [3]. However, one drawback of the quadcopter is that it is inherently unstable, which makes it difficult to control manually [4]. In order to handle this issue, on-board control needs to be used. The obtained performance depends heavily on the measurements from the sensing system. A group of sensors provides information about the quadcopter's status and its surrounding environment, therefore, on-board sensors play a major role in quadcopter research [5]. However, due to the limited payload, the number of onboard sensors that a quadcopter can carry is restricted. If the quadcopter is operated outdoors in a hazardous environment, its maximum payload also depends on the forces and torques by the turbulence. Too much payload may cause the quadcopter to crash. It can therefore be interesting to monitor the payload, to allow the quadcopter to land safely if needed.

[1]Division of Automatic Control, Department of Electrical Engineering, Linköping University, SE-58183 Linköping, Sweden. Email: {du.ho.duc, jonas.linder, gustaf.hendeby, martin.enqvist}@liu.se

In [6], the authors have derived a way to estimate the payload of a quadcopter. The main contribution of this work is to design an aerial grasper and estimate the mass when the quadcopter uses the grasper to carry objects between different positions. Naturally, the mass of the quadcopter system changes when the quadcopter grasps different objects. This change is estimated based on the dynamic equations of the force-linear acceleration and the torque-angular acceleration relations of the quadcopter. The measurements are taken as the quadcopter is perturbed slightly around its hovering position. Recursive least squares estimation is then used to detect the payload change.

An alternative to the approach in [6] is to use an enhanced model of the quadcopter. In [7], a drag-force enhanced model is derived. The drag force is created from the interaction of the propeller with the air stream. Fundamental blade element theory is used to derive the entire dynamic model of a quadcopter. However, the experimental validation of the model is only done for the force model describing the relations between the rotation angles and the translational velocities. Two controllers based on the drag-force enhanced model are proposed. The resulting hardware implementations are only evaluated qualitatively by pointing out that the systems are much easier to fly with these new controllers.

The works of [7] is extended in [8]. An observer is presented and the estimation problem is approached from a different viewpoint: improving the translational velocity and attitude estimates using Inertial Measurement Unit (IMU) measurements. The improvement is due to a better dynamic model that correctly explains the physics related to the measured acceleration. In principle, it is shown that the accelerometers directly measure the translational velocity. However, the model parameters are based on the estimated values of the payload as well as the drag coefficient which are typically obtained using least squares optimization. In order to achieve consistent estimates, this method requires accurate measurements of the signals from a Vicon (Motion Capture) system. Therefore, this approach is usually not applicable when the Vicon system is missing, for example when the quadcopter is operating in outdoor environments.

In this paper, another estimator is designed to detect the change of the mass of the quadcopter. The estimator takes the sensor behavior into consideration and only uses the measurements from the IMU and pilot commands to identify the interesting parameters. Therefore, this approach could be suitable for small quadcopters where number of sensors is restricted.

The paper outline is as follows. In Section II, the dynamic models of the quadcopter are presented, especially focusing

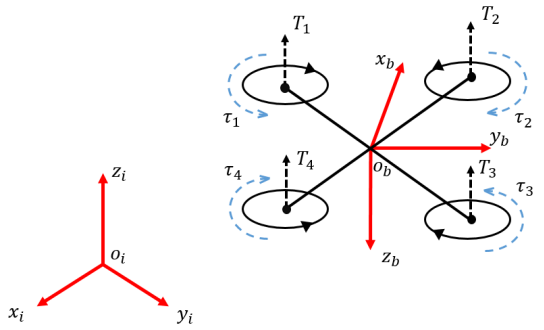

Fig. 1. The inertial and the body coordinate frames of the quadcopter.

on the relation between the roll rate and lateral acceleration. The methods used to estimate the parameters of the model are presented in Section III. The simulation and experimental results are shown in Sections IV and V, respectively, and Section VI concludes the paper.

II. Modeling

In this section, the mathematical equation of the translational model of a quadcopter is presented and a subsystem is considered for the estimation purpose.

A. Quadcopter dynamics

We consider a quadcopter as in Fig. 1. The position of the quadcopter in the inertial frame is defined as $\boldsymbol{\xi}_i = [x_i \quad y_i \quad z_i]^T$. The roll, pitch and yaw angles ϕ, θ and ψ denote the orientation of the quadcopter. These Euler angles are collected in $\boldsymbol{\eta} = [\phi \quad \theta \quad \psi]^T$.

The origin of the body frame is chosen to coincide with the quadcopter's center of mass. In the body frame, the translational velocities are defined as $\boldsymbol{V}_b = [u \quad v \quad w]^T$ and the angular velocities as $\boldsymbol{\nu} = [p \quad q \quad r]^T$.

The rotation matrix describing the relation between the translational velocities in the body-fixed frame and those in the inertial frame is given by

$$\boldsymbol{R} = \begin{bmatrix} C_\theta C_\psi & S_\phi S_\theta C_\psi - C_\phi S_\psi & C_\phi S_\theta C_\psi + S_\phi S_\psi \\ C_\theta S_\psi & S_\phi S_\theta S_\psi + C_\phi C_\psi & C_\phi S_\theta S_\psi - S_\phi C_\psi \\ -S_\theta & S_\phi C_\theta & C_\phi C_\theta \end{bmatrix}, \quad (1)$$

in which $S_x = \sin x$ and $C_x = \cos x$. The rotation matrix $\boldsymbol{R}$ is orthogonal since $\boldsymbol{R}^{-1} = \boldsymbol{R}^T$ where $\boldsymbol{R}^{-1}$ is the rotation matrix from the inertial frame to the body frame.

The quadcopter is assumed to be a rigid body and thus the Newton-Euler equations can be used to describe its dynamics. In the body frame, the equation describing the translational motion of the quadcopter is given by

$$m\dot{\boldsymbol{V}}_b + \boldsymbol{\nu} \times (m\boldsymbol{V}_b) = m\boldsymbol{R}^T\boldsymbol{g} + \boldsymbol{T}_b - \boldsymbol{\lambda}\boldsymbol{V}_b, \quad (2)$$

where the variables and constants are explained in Table I.

The right hand side of (2) contains two key aspects of the quadcopter's dynamics. The second term is the main thrust, which is perpendicular to the rotor plane, and it does not affect the motion of the quadcopter in this frame. The last term is a drag force in the x_b-y_b plane that is caused mainly by a phenomenon called blade flapping [5]. The blade-flapping effect is due to the flexibility of the rotors and occurs primarily when the quadcopter is moving freely in the air. The effect of the relative speed of the blades with respect to free air divides the operating region of the propeller into two areas: a retreating and an advancing blade. The advancing blade has higher relative velocity than the retreating one, which creates a force imbalance between the two areas. This results in a drag force acting in the opposite direction compared to the motion of the quadcopter's body. Luckily, the mathematical expression is simple and a single term is sufficient to represent this effect. This term carries information about the horizontal linear velocities which are revealed in the measurement of the acceleration.

TABLE I

The Notation of the Translational Dynamic Equation.

Symbol	Quantity
m	Mass of the quadcopter $[kg]$
$\dot{\boldsymbol{V}}_b$	Accelerations of the quadcopter $[m/s^2]$
$\boldsymbol{\nu} \times (m\boldsymbol{V}_b)$	The centrifugal force $[N]$
$\boldsymbol{g}$	The gravity vector $[m/s^2]$
$\boldsymbol{R}$	The rotation matrix
$\boldsymbol{T}_b$	The total thrust $[N]$
$\boldsymbol{\lambda}$	The drag coefficient matrix $[Ns/m]$

The above analysis discloses a possibility to design a estimator in order to be able to track mass changes of the quadcopter. Projecting (2) onto the x_b-y_b plane in the body-fixed frame, i.e., assuming $r = 0$ and $w = 0$, yields

$$\dot{u} = -g\sin(\theta) - \frac{\lambda_1}{m}u \quad (3a)$$

$$\dot{v} = g\cos(\theta)\sin(\phi) - \frac{\lambda_1}{m}v. \quad (3b)$$

where λ_1 is the drag coefficient. Interestingly, the above model does not have a standard input such as the thrust or control signal, which might require a non-standard way to address the estimation problem. Furthermore, since the quadcopter is designed symmetrically, the lateral dynamic in the y_b axis is similar to the longitudinal one. Hence, it is sufficient to consider only the roll motion of the quadcopter.

The IMU provides measurements in a sensor-fixed coordinate system of the angular velocities and the linear accelerations in three dimensions. Since the sensor-fixed coordinate frame coincides with the body-fixed frame of the quadcopter except for a 180° rotation around the x_b axis, the lateral acceleration is given by

$$a_y = g\cos(\theta)\sin(\phi) - \dot{v} = \frac{\lambda_1}{m}v, \quad (4)$$

which is proportional to the lateral velocity. Hence, a_y provides information about v, which we can view as the output of the model (3b). The roll rate gyroscope provides $\dot{\phi}$ which can be integrated directly to provide the input ϕ to the model (3b). However, both measurements from the accelerometer and gyroscope are noisy, which leads to an errors-in-variables problem. Another issue is that the disturbances in a_y and $\dot{\phi}$

are correlated with each other under the effect of the closed-loop control. The purpose of this work is to deal with these problems.

B. Linearized model

The lateral model (3b) can be linearized under the small angle assumption ($\sin(\phi) \approx \phi$ and $\cos(\theta) \approx 1$) which gives

$$\dot{v} = g\phi - \frac{\lambda_1}{m} v + \bar{\tau}, \tag{5}$$

where $\bar{\tau}$ represents process noise and unmodeled dynamics.

Combining (4) and the roll rate measurement $\dot{\phi}_s = \dot{\phi} + e_{\dot{\phi}}$ from the measurement model of an IMU gives the transfer function

$$\begin{aligned} a_{y,s} &= a_y + e_y = \frac{\frac{\lambda_1}{m} g}{\mathsf{p}(\mathsf{p} + \frac{\lambda_1}{m})}(\dot{\phi}_s - e_{\dot{\phi}}) + e_y + \bar{\tau} \\ &= \frac{\frac{\lambda_1}{m} g}{\mathsf{p}(\mathsf{p} + \frac{\lambda_1}{m})}\dot{\phi}_s + e, \end{aligned} \tag{6}$$

where $a_{y,s}$ is the measurement of the lateral acceleration and p is the differential operator. Moreover, it should be noted that the total noise term e is colored and that a noise model might be required in the estimation step.

In fact, the measurements are taken in the discrete time domain and they need to be related to the model. Here, the transfer function is discretized using the Bilinear transformation $\mathsf{p} = \frac{2}{T_s}\frac{\mathsf{q}-1}{\mathsf{q}+1}$ which gives

$$a_{y,s}(t) = \beta_1 \frac{\mathsf{q}^2 + 2\mathsf{q} + 1}{\mathsf{q}^2 + \alpha_1 \mathsf{q} + \alpha_2}\dot{\phi}_s(t) + e(t), \tag{7}$$

where

$$\beta_1 = \frac{\frac{\lambda_1}{m} g T_s^2}{4 + 2\frac{\lambda_1}{m} T_s}, \quad \alpha_1 = -\frac{8}{4 + 2\frac{\lambda_1}{m} T_s}, \quad \alpha_2 = \frac{4 - 2\frac{\lambda_1}{m} T_s}{4 + 2\frac{\lambda_1}{m} T_s}, \tag{8}$$

t is the time instant, q is the forward shift operator and T_s is the sample time.

Another way to represent the discrete-time lateral model (7) is to rewrite it on state-space form, taking only the lateral acceleration $a_{y,s}(t)$ as the output. With the state defined as $x(t) = [a_y(t-1) \quad a_y(t)]^T$, the input as $u(t) = \dot{\phi}_s(t+1) + 2\dot{\phi}_s(t) + \dot{\phi}_s(t-1)$ and the output as $y(t) = a_{y,s}(t)$, we get

$$\begin{bmatrix} x_1(t+1) \\ x_2(t+1) \end{bmatrix} = \begin{bmatrix} x_2(t) \\ -\alpha_1 x_2(t) - \alpha_2 x_1(t) + \beta_1 u(t) \end{bmatrix} + \bar{\tau}_x \tag{9a}$$

$$y(t) = x_2(t) + e_y. \tag{9b}$$

The estimate of the discrete-time parameter vector $\vartheta = [\alpha_1 \quad \alpha_2 \quad \beta_1]^T$ gives information about $\frac{\lambda_1}{m}$. Hence, the ratio $a = \frac{\lambda_1}{m}$ can be obtained from the estimated mean $\hat{\vartheta}$ and covariance $P_{\hat{\vartheta}}$ by solving the nonlinear weighted least squares equation [9]

$$\hat{a} = \arg\min_a \left[\hat{\vartheta} - \vartheta(a)\right]^T P_{\hat{\vartheta}}^{-1} \left[\hat{\vartheta} - \vartheta(a)\right], \tag{10}$$

and using Gauss approximation formula [10] to estimate the covariance of $\hat{a}$ as

$$P_{\hat{a}} = \left[\frac{\partial \vartheta^T}{\partial a} P_{\hat{\vartheta}}^{-1} \frac{\partial \vartheta}{\partial a}\right]^{-1}\Big|_{a=\hat{a}}. \tag{11}$$

In this paper, several datasets have been collected. In the first dataset, the mass m is known and the physical parameter λ_1 is estimated. Based on that estimate of λ_1, the change of the mass can be computed using an estimate of the ratio $a = \frac{\lambda_1}{m}$ obtained from a second dataset.

III. Estimation methods

In this section, three mass estimation methods, which can be used to estimate the mass of the quadcopter, are presented.

A. Least-squares estimation

The discrete-time model (7) can be expressed in linear regression form, defining $u(t) = \dot{\phi}_s(t) + 2\dot{\phi}_s(t-1) + \dot{\phi}_s(t-2)$ and $y(t) = a_{y,s}(t)$ as

$$\begin{aligned} y(t) &= \begin{bmatrix} -y(t-1) & -y(t-2) & u(t) \end{bmatrix} \begin{bmatrix} \alpha_1 \\ \alpha_2 \\ \beta_1 \end{bmatrix} + \bar{\tau}_0 \\ &= \varphi^T(t)\vartheta_0 + \bar{\tau}_0, \end{aligned} \tag{12}$$

in which $\varphi(t)$ depends only on the past values of $a_{y,s}(t)$ as well as the past and current values of the input signal $\dot{\phi}_s(t)$, ϑ_0 is the true parameter vector $[\alpha_1 \quad \alpha_2 \quad \beta_1]^T$ and $\bar{\tau}_0$ is the disturbance. The least squares (LS) estimate is given by

$$\hat{\vartheta}_{LS} = \arg\min_{\vartheta} \frac{1}{N}\sum_{t=1}^{N} \|y(t) - \varphi^T(t)\vartheta\|_2^2, \tag{13}$$

which has the analytical solution

$$\begin{aligned} \hat{\vartheta}_{LS} &= \left[\frac{1}{N}\sum_{t=1}^{N} \varphi(t)\varphi^T(t)\right]^{-1} \frac{1}{N}\sum_{t=1}^{N} \varphi(t)y(t) \\ &= R_{\varphi\varphi}^{-1} f_{\varphi y}. \end{aligned} \tag{14}$$

The estimated covariance matrix of the estimated parameters is given by

$$P_{LS} = \hat{\sigma}^2 R_{\varphi\varphi}^{-1}, \tag{15}$$

where $\hat{\sigma}$ is the estimated standard deviation of the residual.

B. Extended Kalman filter

An extended Kalman filter (EKF) can also be used to estimate the unknown parameters by extending the state vector of (9). The augmented state is

$$x_a(t) = \begin{bmatrix} x^T(t) & \frac{\lambda_1}{m} \end{bmatrix}^T. \tag{16}$$

The resulting system is presented as the process and measurement models

$$\begin{aligned} x_a(t+1) &= \underbrace{\begin{bmatrix} x_2(t) \\ -\frac{4-2x_3(t)T_s}{4+2x_3(t)T_s} x_1(t) + \frac{8x_2(t)}{4+2x_3(t)T_s} + \frac{gT_s^2 x_3(t)u(t)}{4+2x_3(t)T_s} \\ x_3(t) \end{bmatrix}}_{f(x,u)} \\ &\quad + \bar{\tau}_{x_a}(t) \\ y(t) &= \underbrace{x_2(t)}_{h(x,u)} + e_y(t). \end{aligned} \tag{17}$$

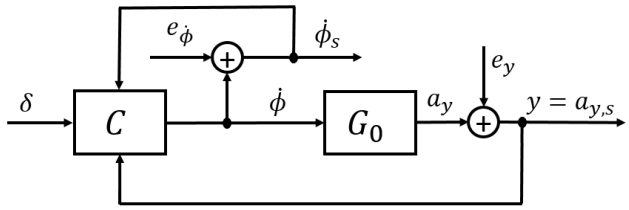

Fig. 2. The closed-loop block diagram of the system (6) with $\bar{\tau} = 0$. The input $\dot{\phi}$ and the output a_y are measured with noises according to Section II. These noises $e_{\dot{\phi}}$ and e_y are correlated with the input signal $\dot{\phi}$ and the output signal a_y due to the problem reformulation and effect of the feedback but are uncorrelated with the reference signal δ.

For initialization, the first two states are set to zero and their variance are set to large positive values, to reflect the uncertainty in the initial state. The third state is initialized using its estimate from the IV method and its variance is also set to a large positive value. The measurement noise covariance matrix is estimated using the first seconds of measurements of the quadcopter prior to takeoff and the process noise variance matrix is tuned manually to achieve the best possible performance of the estimator. The EKF is implemented according to [9].

C. Instrumental variable method

As can be seen in the lateral model (6), the right hand side contains noise that is colored and correlated with the input due to the problem reformulation and the closed-loop setup. Therefore, the conventional LS method might not be able to provide a consistent estimate [10]. To overcome this limitation, one alternative is to use the instrumental variable (IV) method. This method is based on the use of an instrument vector $\xi(t)$ to extract the interesting information from $\dot{\phi}_s$ and $a_{y,s}$.

In this paper, an improved version of the IV method called extended IV is used, where the parameter vector ϑ is obtained by solving

$$\hat{\vartheta}_{IV} = \arg\min_{\vartheta} \frac{1}{N} \sum_{t=1}^{N} \|\xi(t)L(\mathsf{q})y(t) - \xi(t)L(\mathsf{q})\varphi^T(t)\vartheta\|_Q^2, \tag{18}$$

where $\|x\|_Q^2 = x^T Q x$, $Q \geq 0$ is a weighting matrix and $L(\mathsf{q})$ is a stable prefilter.

In principle, the instruments $\xi(t)$ are created as

$$\xi(t) = L(\mathsf{q})\left[\hat{y}_0(t), \cdots \hat{y}_0(t-n_y),\ \hat{u}_0(t), \cdots \hat{u}_0(t-n_u)\right]^T, \tag{19}$$

in which $\hat{u}_0(t)$ and $\hat{y}_0(t)$ are the simulated input and output, respectively. In fact, these simulated signals are generated in a closed-loop setup using the reference signal $\delta(t)$ as

$$\hat{u}_0(t) = \hat{G}_{\delta u}(\mathsf{q}, \hat{\vartheta})\delta(t) \tag{20a}$$

$$\hat{y}_0(t) = \hat{G}_{\delta y}(\mathsf{q}, \hat{\vartheta})\delta(t), \tag{20b}$$

where $\hat{G}_{\delta u}(\mathsf{q}, \hat{\vartheta})$ and $\hat{G}_{\delta y}(\mathsf{q}, \hat{\vartheta})$ are two estimated transfer functions from $\delta(t)$ to $u(t)$ and $y(t)$, respectively. In principle, the true transfer functions could be computed using the controller and the system, depicted in Fig. 2. However, since the true controller as well as the system are unknown, the two transfer functions $\hat{G}_{\delta u}(\mathsf{q}, \hat{\vartheta})$ and $\hat{G}_{\delta y}(\mathsf{q}, \hat{\vartheta})$ are estimated with excessive model orders to ensure that the model set contains the true system.

The choice of the prefilter $L(\mathsf{q})$ is important because it has a considerable effect on the covariance of the estimated parameters [10]. If the true noise model structure is known, the covariance of the estimate can be minimized, which is treated more precisely in [11]. In [12], the authors provide several choices of the pre-filter, the optimal instruments and approximate optimal instruments for a closed-loop system. In this paper, an ARMA noise model is estimated using the residual $\bar{\tau}_0$ as the output and the pre-filter $L(\mathsf{q})$ is chosen as the inverse of the estimated noise model.

The structure of the closed-loop extended IV estimator is typically identical to that of the open-loop one. As a result, the estimated covariance matrix P_{iv} is given as

$$P_{\text{iv}} = \hat{\sigma}^2 \left(R_{\xi\bar{\varphi}}^T Q R_{\xi\bar{\varphi}}\right)^{-1} R_{\xi\bar{\varphi}}^T Q R_{\xi\xi} Q R_{\xi\bar{\varphi}} \left(R_{\xi\bar{\varphi}}^T Q R_{\xi\bar{\varphi}}\right)^{-1}, \tag{21}$$

where $R_{\xi\bar{\varphi}} = \mathbb{E}\left[\xi(t)\bar{\varphi}^T(t)\right] = \mathbb{E}[\xi(t)L(\mathsf{q})\varphi^T]$, $R_{\xi\xi} = \mathbb{E}[\xi(t)\xi(t)^T]$ and $\hat{\sigma}$ is the estimated standard deviation of the residual. The IV algorithm implemented in this paper is similar to the one in [13].

TABLE II

THE COEFFICIENTS OF THE TWO NOISE MODELS $H_{\dot{\phi}_s}(\mathsf{q})$ AND $H_{a_{y,s}}(\mathsf{q})$.

Order	$H_{\dot{\phi}_s}(\mathsf{q})$		$H_{a_{y,s}}(\mathsf{q})$	
	Numerator	Denominator	Numerator	Denominator
z^6	0.449	1	0.4137	1
z^5	0.277	1.604	0.3991	1.359
z^4	0.02359	0.818	0.4962	0.5101
z^3	0.8013	0.4226	1.239	0.1654
z^2	0.4817	0.2457	0.6176	0.1182
z^1	−0.03697	0.03886	−0.0115	0.04615
z^0	0.08703	0.03612	0.09951	0.05472

IV. SIMULATION RESULTS

In order to evaluate the abilities of the three estimation approaches, a Monte Carlo (MC) simulation has been conducted for the quadcopter's lateral dynamics (7). For each individual MC simulation, three datasets corresponding to the nominal mass and two additional masses have been generated in Simulink with the sample rate of 200 Hz. Each dataset contains 11000 samples simulating 55 s of flight.

The simulation has been repeated 100 times with different noise realizations for $\dot{\phi}_s$ and $a_{y,s}$. Each realization is created by feeding a white noise signal with standard deviation of 0.1 through a filter of order 6. The coefficients of the noise models of $\dot{\phi}_s$ and $a_{y,s}$ are chosen to capture approximately the dominant frequencies estimated from the spectrum of the experimental signals and are given in Table II. The order of the noise model is then selected to 6.

The true value of the drag coefficient is chosen as 0.36, while the nominal mass of the quadcopter is set to 455 g and two additional masses are 510 g and 582 g, respectively.

TABLE III

THE AVERAGE OF THE ESTIMATED λ_1 WITH STANDARD DEVIATION BASED ON THE MC SIMULATIONS. THE FIRST COLUMN INDICATES THE MASS SETUP WHILE THE ESTIMATION RESULTS ARE SHOWN IN THE $2^{\text{ND}} - 4^{\text{TH}}$ COLUMNS.

True mass	LS	EKF	IV
$455g$	818.3 ± 20.34	0.3598 ± 0.0543	0.3605 ± 0.0043
$510g$	916.9 ± 22.77	0.3596 ± 0.0639	0.3605 ± 0.0052
$582g$	1043.7 ± 25.88	0.3593 ± 0.0769	0.3611 ± 0.0062

TABLE IV

THE ROOT MEAN SQUARE ERROR OF THE ESTIMATES OF λ_1 BASED ON THE MC SIMULATIONS. THE FIRST COLUMN INDICATES THE MASS SETUP WHILE THE ESTIMATION RESULTS ARE SHOWN IN THE $2^{\text{ND}} - 4^{\text{TH}}$ COLUMNS.

True mass	LS	EKF	IV
$455g$	818.2	0.0043	0.0043
$510g$	916.5	0.0051	0.0047
$582g$	1043.4	0.0053	0.0047

Fig. 3 shows the signals in one typical dataset. The reference signal $\delta(t)$ is created in such a way that the quadcopter is supposed to move similarly to the experiments in Section V. However, since the controller of the quadcopter is not simulated in this setup, the simulated system is more simple than the real one.

The estimates of λ_1 are given in Table III. It turns out that the values obtained from the LS method are far from the true values. For the EKF method, since it is a recursive approach for estimating the state and parameters simultaneously, it is natural that it gives a different result compared to the LS and IV methods where the whole batch of measurements is used to estimate the interesting parameters. However, since the physical parameter λ_1 is supposed to be constant during the experiment, the last estimated state vector and state covariance from the EKF estimator in each MC simulation is used to compute the mean and covariance of λ_1. More precisely, the obtained value of λ_1 from the EKF is slightly worse than the IV result for the three different mass setups.

The simulation results can also been analyzed using the root mean square error (RMSE) of the estimated λ_1 in Table IV. The smallest root mean square errors in all three mass setups are achieved by the IV estimator.

TABLE V

THE AVERAGE OF THE ESTIMATED MASSES AND THE APPROXIMATED STANDARD DEVIATION USING THE RATIO $\frac{\lambda_1}{m}$ BASED ON THE MC SIMULATIONS. FOR EACH MC SIMULATION, THE MASS $\hat{m}_{c,i}$ IS ESTIMATED AS $\hat{m}_{c,i} = \frac{\hat{\lambda}_{1,m_{ref},i}}{\hat{a}_{c,i}}$ AND THE COVARIANCE OF $\hat{m}_{c,i}$ IS APPROXIMATED WITH $P_{\hat{m}_{c,i}} = (P_{\hat{\lambda}_{1,m_{ref},i}}\hat{a}^2_{c,i} + \hat{\lambda}^2_{1,m_{ref},i}P_{\hat{a}_{c,i}})/\hat{a}^4_{c,i}$ FOR THE LS AND IV METHODS.

m_{ref}	m_c	$\hat{m}_c$ (LS)	$\hat{m}_c$ (EKF)	$\hat{m}_c$ (IV)
$455g$	$510g$	$455.2 \pm 16.0g$	$510.4 \pm 119.1g$	$510.1 \pm 9.6g$
	$582g$	$456.4 \pm 16.1g$	$583.0 \pm 152.8g$	$581.1 \pm 12.2g$
$510g$	$455g$	$510.0 \pm 17.9g$	$454.8 \pm 106.0g$	$455.1 \pm 8.5g$
	$582g$	$511.4 \pm 17.9g$	$582.6 \pm 162.1g$	$581.1 \pm 13.2g$
$582g$	$455g$	$580.5 \pm 20.4g$	$454.4 \pm 119.1g$	$455.8 \pm 9.6g$
	$510g$	$580.6 \pm 20.4g$	$509.7 \pm 141.8g$	$510.9 \pm 10.6g$

TABLE VI

THE ROOT MEAN SQUARE ERROR OF THE MASS ESTIMATES BASED ON THE MC SIMULATIONS. FOR EACH MC SIMULATION, THE MASS $\hat{m}_{c,i}$ IS COMPUTED AS $\hat{m}_{c,i} = \frac{\hat{\lambda}_{1,m_{ref},i}}{\hat{a}_{c,i}}$ AND $RMSE = \sqrt{\frac{1}{N}\sum_{i=1}^{N}(\hat{m}_{c,i} - m_c)^2}$, WHERE N IS THE NUMBER OF MC SIMULATIONS.

m_{ref}	m_c	RMSE (LS)	RMSE (EKF)	RMSE (IV)
$455g$	$510g$	55.7	9.4	9.0
	$582g$	129.0	10.3	9.8
$510g$	$455g$	56.1	8.3	8.0
	$582g$	71.3	11.7	10.5
$582g$	$455g$	126.2	8.0	7.7
	$510g$	71.6	10.3	9.3

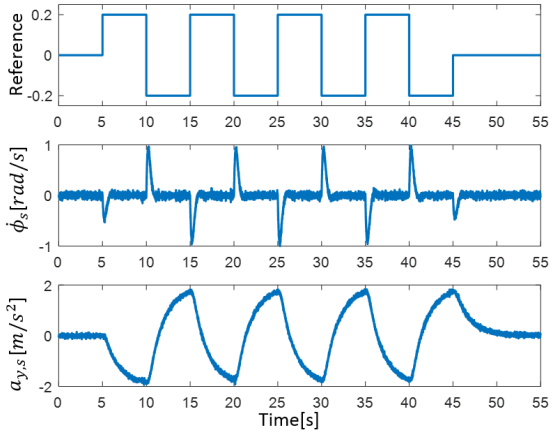

Fig. 3. An example of the simulated data. The reference signal $\delta(t)$ is found in the top sub-figure, the roll rate $\dot{\phi}_s$ in the middle one and the bottom sub-figure shows the lateral acceleration $a_{y,s}$.

Table V shows the estimates of the mass using the ratio $\frac{\lambda_1}{m}$. In fact, six mass estimation setups are obtained using three datasets corresponding with three different mass setups of the quadcopter. For each combination, the mass $\hat{m}_c$ and its standard deviation are computed using estimates of two ratios $a_{ref} = \frac{\lambda_{1,m_{ref}}}{m_{ref}}$ and $a_c = \frac{\lambda_{1,m_c}}{m_c}$. With a known m_{ref}, the mass $\hat{m}_c$ is estimated as $\hat{m}_c = \frac{\hat{\lambda}_{1,m_{ref}}}{\hat{a}_c}$ where $\hat{\lambda}_{1,m_{ref}}$ and $\hat{a}_c$ are the estimated values of $\lambda_{1,m_{ref}}$ and $\frac{\lambda_{1,m_c}}{m_c}$, respectively. The approximated covariance $P_{\hat{m}_c}$ of $\hat{m}_c$ is computed using the Gauss approximation formula, $P_{\hat{m}_c} = (P_{\hat{\lambda}_{1,m_{ref}}}\hat{a}_c^2 + \hat{\lambda}^2_{1,m_{ref}}P_{\hat{a}_c})/\hat{a}_c^4$. In detail, the LS method provides a biased estimate of λ_1 that results in a failure to detect the variation of the masses. The EKF and IV methods, on the other hand, provide accurate mass estimates. However, since the standard deviation of the λ_1 estimate affects that of the mass estimate, the IV estimator also provides the smallest standard deviation of the mass estimates in all combinations.

The RMSE of the mass estimates is shown in Table VI. The LS method gives the worst results due to the inaccurate

Fig. 4. AR Drone.

estimate of λ_1. The IV method, on the other hand, gives a bit smaller RMSE of the mass estimate than the EKF.

V. Experimental results

In this section, the experimental results using an AR Drone are presented. The experiments have been performed with several mass setups.

A. AR Drone

The Parrot AR Drone 2 is a popular quadcopter platform for research and education. It consists of a carbon-fiber structure, a plastic body, four high-efficiency brushless motors, sensors and a control board, two cameras and a removable hull, see Fig. 4. The maximum translational speed of the quadcopter is 5 m/s and its battery provides enough energy for up to 13 minutes of continuous flight. The AR Drone is capable to communicate with the ground workstation via Wi-Fi, which lets the user control the vehicle with an external device. Moreover, the Wi-Fi communication provides the access to preprocessed sensor measurements and images from onboard cameras stored in the transmitted messages.

B. Mass estimation

During the experiment, the first seconds of measurements are used to estimate the bias of IMU when the AR Drone is on the ground. Afterwards, the AR Drone is flying and excited from the hovering position to move left-right with constant altitude and zero pitch angle. Fig. 5 illustrates a typical dataset collected in the particular experiments. In the figure, the bias estimates are already subtracted from the measurements.

Three datasets have been collected, one with the nominal mass and two with different additional masses. The nominal mass of the AR Drone is 455 g while the new masses (nominal + additional) are 510 g and 582 g. These small additional masses are separated equally into four pieces placed underneath the propellers to ensure that they influence the aerodynamic of the quadcopter as little as possible.

Table VII shows the estimate of λ_1 with its standard deviation. Note that λ_1 is an unknown parameter. However, due to the small deviations of the λ_1 estimates and the mass estimates in Table VIII for the IV algorithm, it is reasonable to believe that the obtained value of λ_1 from the IV method is actually close to the truth. In contrast, the LS

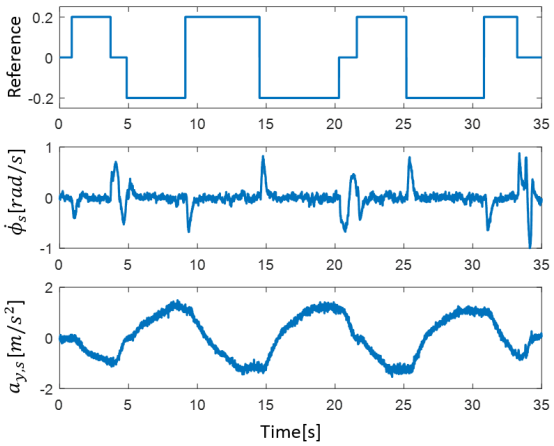

Fig. 5. An example of the experimental data. The top plot shows the reference signal $\delta(t)$ while the lower plots show the roll angular speed $\dot{\phi}_s$ and the lateral acceleration $a_{y,s}$, respectively.

TABLE VII

The estimated λ_1 with standard deviation using experimental data. The first column indicates the mass setup while the estimation results are shown in the $2^{\text{ND}} - 4^{\text{TH}}$ columns.

True mass	LS	EKF	IV
$455g$	935.6 ± 29.3	0.3589 ± 0.1147	0.3599 ± 0.0021
$510g$	350.2 ± 8.9	0.3620 ± 0.1447	0.3641 ± 0.0017
$582g$	256.1 ± 5.1	0.5440 ± 0.1482	0.3607 ± 0.0009

method gives very large values of the drag coefficient, which is unrealistic. The EKF method provides a result similar to the IV method in the first two datasets. However, the estimate of λ_1 in the third dataset is not close to the first two even though the tuning parameters are kept as $R = 0.05$ and $Q = \text{diag}([0.000125 \quad 0.9031 \quad 0.000125]) \times 10^{-6}$ for the three datasets.

The estimate of λ_1 is then used to detect the mass change of the quadcopter. Table VIII shows the mass estimate with its standard deviation in six different setups. For each setup, two estimated ratios of $a_{ref} = \frac{\lambda_{1,m_{ref}}}{m_{ref}}$ and $a_c = \frac{\lambda_{1,m_c}}{m_c}$ are used to compute $\hat{m}_c$ and its standard deviation. Note that the LS estimator provides inaccurate estimates of λ_1 in the three

TABLE VIII

The estimated masses and the approximated standard deviation using the ratio $\frac{\lambda_1}{m}$ and the experimental data. The mass $\hat{m}_c$ is estimated as $\hat{m}_c = \frac{\hat{\lambda}_{1,m_{ref}}}{\hat{a}_c}$ and the covariance of $\hat{m}_c$ is approximated with $P_{\hat{m}_c} = (P_{\hat{\lambda}_{1,m_{ref}}} \hat{a}_c^2 + \hat{\lambda}_{1,m_{ref}}^2 P_{\hat{a}_c})/\hat{a}_c^4$ for the LS and IV methods.

m_{ref}	m_c	$\hat{m}_c$ (LS)	$\hat{m}_c$ (EKF)	$\hat{m}_c$ (IV)
$455g$	$510g$	$1362.5 \pm 54.9g$	$505.6 \pm 258.8g$	$504.1 \pm 3.9g$
	$582g$	$2126.2 \pm 78.9g$	$384.4 \pm 161.2g$	$580.9 \pm 3.8g$
$510g$	$455g$	$170.3 \pm 6.9g$	$458.9 \pm 234.8g$	$460.3 \pm 3.4g$
	$582g$	$795.8 \pm 25.7g$	$387.3 \pm 187.3g$	$587.5 \pm 3.2g$
$582g$	$455g$	$124.5 \pm 4.6g$	$689.7 \pm 289.6g$	$456.1 \pm 3.0g$
	$510g$	$373.1 \pm 12.1g$	$766.4 \pm 370.7g$	$505.2 \pm 2.8g$

datasets. Hence, it fails to detect the mass change of the quadcopter. The EKF estimator is also unable to detect the changes in mass. The best performance is achieved with the IV estimator in which the mass changes are detected successfully in all six combinations.

VI. CONCLUSIONS

An approach for mass estimation of a quadcopter has been presented and validated with simulations and experimental data. The dynamic sub-model describing the relation between the roll rate and lateral acceleration of the quadcopter has been studied. The simulated data is generated using the same scenario as in the real experiments. The measurements used for the estimation are taken from the IMU.

To investigate the possibilities to estimate a mass change, a comparison has been carried out with three estimation methods. It has been shown that the IV method provides accurate estimates of the change of mass while the LS and EKF methods are unreliable, indicating that the IV method outperforms the other methods in this closed-loop setup.

Future work could be to extend the current framework to estimate other interesting parameters of the quadcopter such as the moment of inertia or the center of mass, which is definitively useful for control as well as for fault detection purposes.

ACKNOWLEDGMENT

This project has received funding from the European Union's Horizon 2020 research and innovation programme under the Marie Sklodowska-Curie grant agreement No. 642153.

REFERENCES

[1] G. Cai, B. M. Chen, and T. H. Lee, "An overview on development of miniature unmanned rotorcraft systems," *Frontiers of Electrical and Electronic Engineering in China*, vol. 5, no. 1, pp. 1–14, 2010.

[2] F. Fraundorfer, L. Heng, D. Honegger, G. H. Lee, L. Meier, P. Tanskanen, and M. Pollefeys, "Vision-based autonomous mapping and exploration using a quadrotor MAV," in *2012 IEEE/RSJ International Conference on Intelligent Robots and Systems*, Vilamoura, Algarve, Portugal, Oct 2012, pp. 4557–4564.

[3] C. Bills, J. Chen, and A. Saxena, "Autonomous MAV flight in indoor environments using single image perspective cues," in *2011 IEEE International Conference on Robotics and Automation*, Shanghai, China, May 2011, pp. 5776–5783.

[4] M. D. Hua, T. Hamel, P. Morin, and C. Samson, "Introduction to feedback control of underactuated VTOL vehicles: A review of basic control design ideas and principles," *IEEE Control Systems*, vol. 33, no. 1, pp. 61–75, Feb 2013.

[5] R. Mahony, V. Kumar, and P. Corke, "Multirotor aerial vehicles: Modeling, estimation, and control of quadrotor," *IEEE Robotics Automation Magazine*, vol. 19, no. 3, pp. 20–32, Sept 2012.

[6] D. Mellinger, Q. Lindsey, M. Shomin, and V. Kumar, "Design, modeling, estimation and control for aerial grasping and manipulation," in *2011 IEEE/RSJ International Conference on Intelligent Robots and Systems*, San Francisco, California, USA, Sept 2011, pp. 2668–2673.

[7] P. Martin and E. Salaun, "The true role of accelerometer feedback in quadrotor control," in *Proceedings for the 2010 IEEE International Conference on Robotics and Automation*, Anchorage, USA, 2010, pp. 1623–1629.

[8] R. C. Leishman, J. C. Macdonald, R. W. Beard, and T. W. McLain, "Quadrotors and accelerometers: State estimation with an improved dynamic model," *IEEE Control Systems Magazine*, vol. 34, no. 1, pp. 28–41, 2014.

[9] F. Gustafsson, *Statistical sensor fusion*. Studentlitteratur, 2010.

[10] L. Ljung, *System identification - Theory for the User*, 2nd ed. Prentice-Hall, 1999.

[11] M. Gilson and P. M. J. Van den Hof, "Instrumental variable methods for closed-loop system identification," *Automatica*, vol. 41, no. 2, pp. 241–249, 2005.

[12] M. Gilson, H. Garnier, P. Y. Young, and P. M. J. Van den Hof, "Optimal instrumental variable method for closed-loop identification," *IET Control Theory & Applications*, vol. 5, no. 10, pp. 1147–1154, 2011.

[13] J. Linder, M. Enqvist, and F. Gustafsson, "A Closed-loop Instrumental Variable Approach to Mass and Center of Mass Estimation Using IMU Data," in *53rd IEEE Conference on Decision and Control*, Los Angeles, California, USA, December 2014.